Team Apache Stealth: IMU Attitude Estimation

Ankit Mittal
Department of Robotics Engineering
Worcester Polytechnic Institute
Email: amittal@wpi.edu

Rutwik Kulkarni
Department of Robotics Engineering
Worcester Polytechnic Institute
Email: rkulkarni1@wpi.edu

***Abstract*—This report attempts to explain attitude estimation techniques for orientation determination using data from a 6 DoF (3-DoF gyroscope + 3-DoF accelerometer) Inertial Measurement Unit. Four main approaches are investigated: accelerometer-based estimation, gyroscope-based estimation, complementary filter blending of both accelerometer and gyroscope data, and Madgwick Filter. To enhance the validity of our findings, we have introduced Vicon data as the benchmark, serving as the ground truth against which we evaluate the accuracy of the attitude estimates produced by the different approaches. It is seen that a Madgwick The filter gives the best performance of all.**

I. Introduction

In aerial robotics applications, precise determination of a system's orientation is crucial for providing feedback to autopilot systems or controllers. The Inertial Measurement Unit (IMU) serves as a favored sensor for this purpose, comprising triaxis gyroscopes and accelerometers. Gyroscopes gauge angular velocity, allowing integration over time to approximate orientation. Nonetheless, this numerical integration is vulnerable to accumulating errors, leading to gradual divergence from the true orientation. Conversely, accelerometers measure the Earth's gravitational field, yielding orientation estimates within an absolute frame of reference. Yet, any translational motion distorts gravity measurements, resulting in compromised orientation estimates. This challenge is effectively addressed using a Madgwick filter, which blends accelerometer and gyroscope data from the IMU to yield a unified orientation estimate.
Link To Videos: **Click Here**

II. Data Pre-pocessing

This section outlines the methodologies employed to estimate and rectify biases, as well as scale the raw data values obtained from the IMU into SI units for both the accelerometer and gyroscope sensors.

A. Accelerometer IMU Data

Prior to analysis, the data extracted from the IMU necessitates preprocessing to both convert it into meaningful physical units and counteract any inherent instrumentation bias. The subsequent expression explains the conversion process of raw accelerometer readings, denoted as $a = [a_x \ a_y \ a_z]^T$, into acceleration data represented in m/s^2.

$$\hat{a_i} = 9.81((a_i \times s_{a,i}) + b_{a,i})$$

Here $\hat{a_i}$ represents a_i in physical units, b_{a_i} represents bias and s_{a_i} represents the scale factor for i^{th} axis. Where $i \in x, y, z$ axis.

B. Gyroscope IMU Data

Similarly, the data originating from the gyroscopes underwent processing to convert the raw gyro angular velocity reading $\omega = [\omega_x \ \omega_y \ \omega_z]^T$ into angular velocity data in rad/s, the following expression is used.

$$\hat{\omega_i} = \frac{3300}{1023} \times \frac{\pi}{180} \times 0.3 \times (\omega_i - b_{g,i})$$

To compute the bias term, the average of the initial 200 gyroscope measurements is derived. This assumption is based on the stability of the gyroscope during the initial 200 measurements within each dataset, which is utilized to establish the initial angular velocities. For each axis bias term is determined. Where $k = 200$.

$$b_{g,i} = \frac{1}{k}\sum_{i=1}^{k}\omega_i$$

III. Orientation Determination

In this section, we have addressed the methodology for ascertaining orientation from separately preprocessed accelerometer and gyroscope data. By leveraging the strengths of each sensor, we have formulated the implementation of a complementary filter. This filter integrates the favorable aspects of both datasets to generate an enhanced orientation estimation. Finally, the orientation obtained through the implemented methods is compared with the ground truth observations extracted from the Vicon dataset.

A. Orientation from accelerometer

The estimated orientation values were derived from the accelerometer data by determining how the acceleration vector aligns with the familiar orientation of the gravitational vector. This estimation was achieved using following simple trigonometric relationships.

$$Roll(\phi) = tan^{-1}(a_y/\sqrt{(a_x)^2 + (a_z)^2})$$
$$Pitch(\theta) = tan^{-1}(a_x/\sqrt{(a_y)^2 + (a_z)^2})$$
$$Yaw(\psi) = tan^{-1}(\sqrt{(a_x)^2 + (a_y)^2}/a_z)$$

However, it's crucial to acknowledge that this method of attitude estimation has limitations. Because of the symmetry of the gravity vector around the z-axis, this approach is inherently imprecise for Yaw measurements. Moreover, distinguishing between acceleration stemming from rapid movement and that resulting from gravity is challenging. As a result, this method isn't suitable for offering accurate estimates during swift motions over brief time intervals.

B. Orientation from Gyroscope

The gyroscope values are integrated to obtain the angles. The integration is performed using quaternions due to their inherent advantages in representing orientation changes. Unlike Euler angles, quaternions do not suffer from gimbal lock, which is a phenomenon where a particular orientation configuration limits the range of motion in certain directions. This makes quaternions more robust for continuous rotations. Quaternions comprise of a single real element (represented by the subscript 0) and three imaginary elements (represented by the subscripts 1, 2, and 3). The following expression describes the attitude quaternion.

$$q = [q_0\ q_1\ q_2\ q_3]^T$$
$${q_0}^2 + {q_1}^2 + {q_2}^2 + {q_3}^2 = 1$$

The updated quaternions is calculated as below:

$$\alpha\Delta = |\vec{\omega_k}|\Delta t$$
$$\vec{e}\Delta = \frac{\vec{\omega_k}}{|\vec{\omega_k}|}$$
$$q_k = \left(cos\left(\frac{\alpha\Delta}{2}\right), \vec{e}\Delta sin\left(\frac{\alpha\Delta}{2}\right)\right)$$

To calculate current state quaternion the following equations are used:

$$\alpha = |\vec{\omega_k}|$$
$$\vec{e} = \frac{\vec{\omega_k}}{|\vec{\omega_k}|}$$
$$q_k = \left(cos\left(\frac{\alpha}{2}\right), \vec{e}sin\left(\frac{\alpha}{2}\right)\right)$$

Now, the new state quaternion is described as (k is the current state and k + 1 is the next state),

$$q_{k+1} = q_k q\Delta$$

Then euler angles are calculated from the quaternions as follows:

$$Roll(\phi) = tan^{-1}\left(\frac{2(q_0q_1 + q_2q_3)}{1 - 2({q_1}^2 + {q_2}^2)}\right)$$
$$Pitch(\theta) = sin^{-1}(2(q_0q_2 - q_3q_1))$$

$$Yaw(\psi) = tan^{-1}\left(\frac{2(q_0 q_3 + q_1 q_2)}{1 - 2({q_2}^2 + {q_3}^2)}\right)$$

This method generally performs well, but offers no way to compensate for noise in the IMU readings, therefore the estimates tend to drift and become more inaccurate with time.

IV. Complementry Filter

Following the independent calculation of attitude using accelerometer and gyroscope data, the derived attitudes can be merged to enhance the overall attitude estimation. The complementary filter employs a predetermined weighted average of both individual components to produce a refined attitude estimation. This blending of accelerometer and gyroscope information optimally leverages the strengths of each source to yield a more accurate and stable attitude representation.

$$\begin{bmatrix}\phi\\ \theta\\ \psi\end{bmatrix}_{\text{Comp}} = \begin{bmatrix}\alpha & 0 & 0\\ 0 & \beta & 0\\ 0 & 0 & \gamma\end{bmatrix} \cdot \begin{bmatrix}\phi\\ \theta\\ \psi\end{bmatrix}_{\text{Acc}} + \begin{bmatrix}1-\alpha & 0 & 0\\ 0 & 1-\beta & 0\\ 0 & 0 & 1-\gamma\end{bmatrix} \cdot \begin{bmatrix}\phi\\ \theta\\ \psi\end{bmatrix}_{\text{Gyro}}$$

Here α, β and γ are the mixing parameters. α was chosen as 0.75, β was chosen as 0.75 and γ was chosen as 0.0 . Effectively the gyro measurements are high pass filtered to remove drift and accelerometer measurements are low pass filtered to remove noise.

V. Madgwick Filter

Sebastian Madgwick introduced an orientation filter designed for IMUs containing tri-axial gyroscopes and [1]. This filter utilizes a quaternion-based representation of orientation to accurately depict three-dimensional orientations, avoiding the problematic singularities encountered with Euler angle representations. This approach enables the utilization of accelerometers within an analytically derived and optimized gradient-descent algorithm. This algorithm calculates the quaternion derivative that characterizes the gyroscope measurement error direction.

A. Orientation increment from accelerometer

In order to derive the attitude quaternion $\hat{q}$ from the gravitational acceleration vector g and the data from a 3-axis accelerometer sensor, which supplies gravity vector information in the body frame as a_x, a_y, and a_z, an optimization problem is structured as outlined below.

$$\min_{{}^I_W\hat{q}\in\mathbb{R}^{4\times 1}} f({}^I_W\hat{q}, {}^W\hat{g}, {}^I\hat{a}) \tag{1}$$

$$f({}^I_W\hat{q}, {}^W\hat{g}, {}^I\hat{a}) = {}^I_W\hat{q}^* \otimes {}^W\hat{g} \otimes {}^I_W\hat{q} - {}^I\hat{a} \tag{2}$$

where,

$${}^I\hat{a} = [0\ a_x\ a_y\ a_z]^T$$

$${}^W\hat{g} = [0\ 0\ 0\ 1]^T$$

Here q^* denotes the conjugate of q and $\otimes$ denotes the quaternions multiplication. And ${}^I\hat{a}$ and ${}^W\hat{g}$ are normalized vectors.

The solution to the above problem can be computed using the gradient descent algorithm and increment change can be calculated as follows:

$$\nabla f({}^I_W\hat{q}_{est,t}, {}^W\hat{g}, {}^I\hat{a}_{t+1}) = J^T({}^I_W\hat{q}_{est,t}, {}^W\hat{g}) f({}^I_W\hat{q}_{est,t}, {}^W\hat{g}, {}^I\hat{a}_{t+1}) \tag{3}$$

$$\nabla f({}^I_W\hat{q}_{est,t}, {}^W\hat{g}, {}^I\hat{a}_{t+1}) = \begin{bmatrix}2(q_2q_4 - q_1q_3) - a_x\\ 2(q_1q_2 + q_3q_4) - a_y\\ 2(\frac{1}{2} - q_2^2 - q_3^2) - a_z\end{bmatrix} \tag{4}$$

$$J^T({}^I_W\hat{q}_{est,t}, {}^W\hat{g}) = \begin{bmatrix}-2q_3 & 2q_4 & -2q_1 & 2q_2\\ 2q_2 & 2q_1 & 2q_4 & 2q_3\\ 0 & -4q_2 & -4q_3 & 0\end{bmatrix} \tag{5}$$

$${}^I_W\hat{q}_{\nabla,t+1} = -\beta\frac{\nabla f({}^I_W\hat{q}_{est,t}, {}^W\hat{g}, {}^I\hat{a}_{t+1})}{||\nabla f({}^I_W\hat{q}_{est,t}, {}^W\hat{g}, {}^I\hat{a}_{t+1})||} \tag{6}$$

Here β can be considered as a step size or a tunable trade-off parameter that determines when the gyro has to take over the acc.

B. Orientation increment from gyro

The rate of change of the attitude quaternion ${}^{I}_{W}\dot{q}_{\omega,t+1}$ can be calculated from the measured 3-axis gyroscope angular velocities ω_x, ω_y, ω_z and the current quaternion estimate ${}^{I}_{W}\hat{q}_{est,t}$ as follows.

$$ {}^{I}_{W}\dot{q}_{\omega,t+1} = \frac{1}{2}\, {}^{I}_{W}\hat{q}_{est,t} \otimes [0,\ {}^{I}\omega_{t+1}]^T \tag{7} $$

C. Fuse Measurements

The increments calculated from the accelerometer and gyro are fused together to obtain the estimated attitude ${}^{I}_{W}\hat{q}_{est,t+1}$

$$ {}^{I}_{W}\dot{q}_{est,t+1} = I_W\dot{q}_{\omega,t+1} + {}^{I}_{W}\, q_{\nabla,t+1} \tag{8} $$

$$ {}^{I}_{W}q_{est,t+1} = {}^{I}_{W}\, \hat{q}_{est,t} + {}^{I}_{W}\, \dot{q}_{est,t+1}\Delta t \tag{9} $$

Here,Δt is the time elapsed between the timestamp t and $t+1$. The initial attitude ${}^{I}_{W}\hat{q}_{est,t=0}$ estimation is assumed that the device is at rest.

All the above steps of orientation increment from the accelerometer, orientation increment from the gyroscope, and measurement fusion are repeated at each timestamp. It must be noted that resultant ${}^{I}_{W}q_{est,t+1}$ quaternion moves out of the unit quaternion space and thus they no longer represent the attitude/orientation of the body. To rectify this they must be normalized to ${}^{I}_{W}\hat{q}_{est,t+1}$ after every iteration that they are calculated.

VI. Result

Plots depicting the calculated Roll (ϕ), Pitch (θ), and Yaw (ψ) obtained from various methods are generated for each dataset (1 to 6). These methods encompass individual accelerometer and gyroscope readings, complementary filter as well as the Madgwick filter. In order to evaluate their accuracy, the Vicon measurements are regarded as the established ground truth against which the performance of each method is assessed. The evaluated dataset from 6 to 10 are test datasets and do not contain Vicon measurements

VII. Conclusion

The results demonstrate varying accuracy among different attitude estimation methods, with the madgwick filter showing the closest alignment to Vicon truth data. While roll and pitch are well-estimated across all methods, yaw suffers due to accelerometer limitations. Gyro-based estimation is prone to drift as integration errors accumulate with time. This affects combined methods, especially yaw where accelerometer correction for gyro drift is absent.Consequently, the combined and Madgwick filters exhibited fluctuating performance, especially in the yaw axis, where the accelerometer lacked the ability to furnish any orientation estimate for the correction of gyro drift. While the Madgwick filter may not offer a flawless attitude estimate, it demonstrates robustness by effectively mitigating the impact of gyro reading errors and handling discontinuities in raw data without compromising orientation tracking accuracy. Additionally, the Madgwick filter boasts a relatively straightforward implementation and minimal computational overhead, positioning it as a superior choice compared to other attitude estimation methods explored.

Acknowledgment

The author would like to thank Prof. Nitin Sanket and the TA of this course RBE595.

References

[1] Sebastian Madgwick, Samuel Wilson, Ruth Turk, Jane Burridge, Christos Kapatos, and Ravi Vaidyanathan. An extended complementary filter (ecf) for full-body marg orientation estimation. *IEEE/ASME Transactions on Mechatronics*, PP:1–1, 05 2020.

1. TRAIN DATASET 1

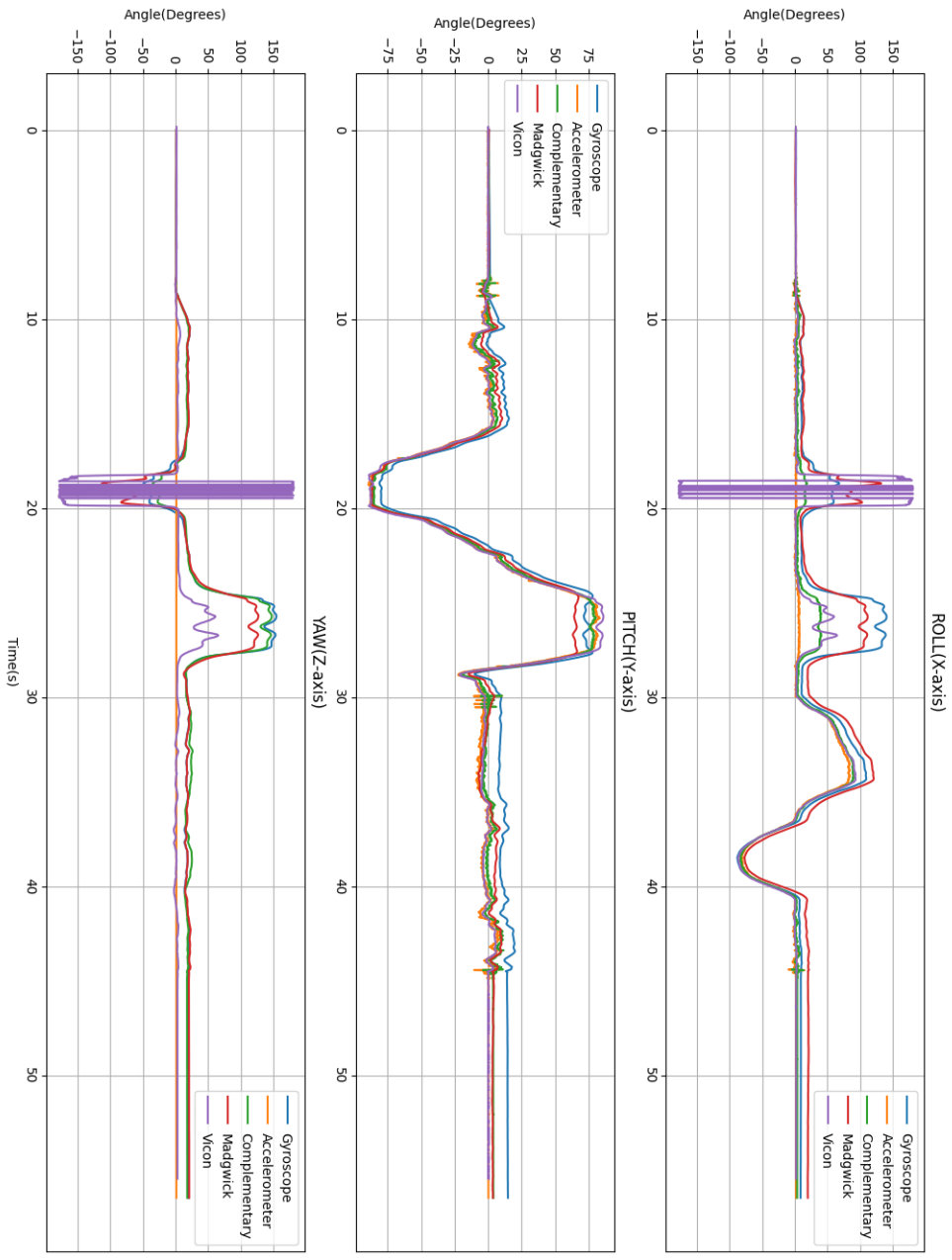

Fig. 1: Comparison of Attitude Estimations for dataset 1

2. TRAIN DATASET 2

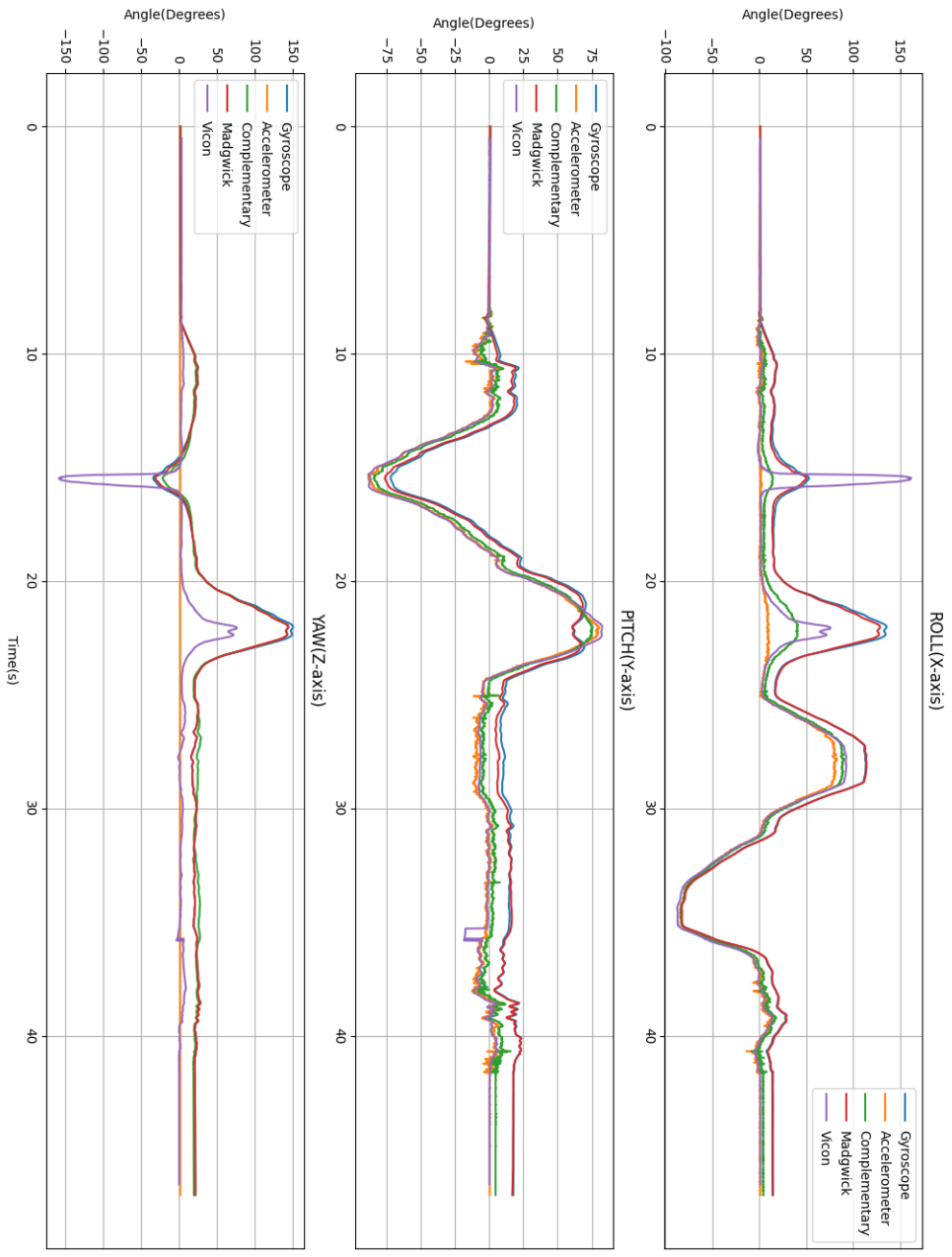

Fig. 2: Comparison of Attitude Estimation for dataset 2

3. TRAIN DATASET 3

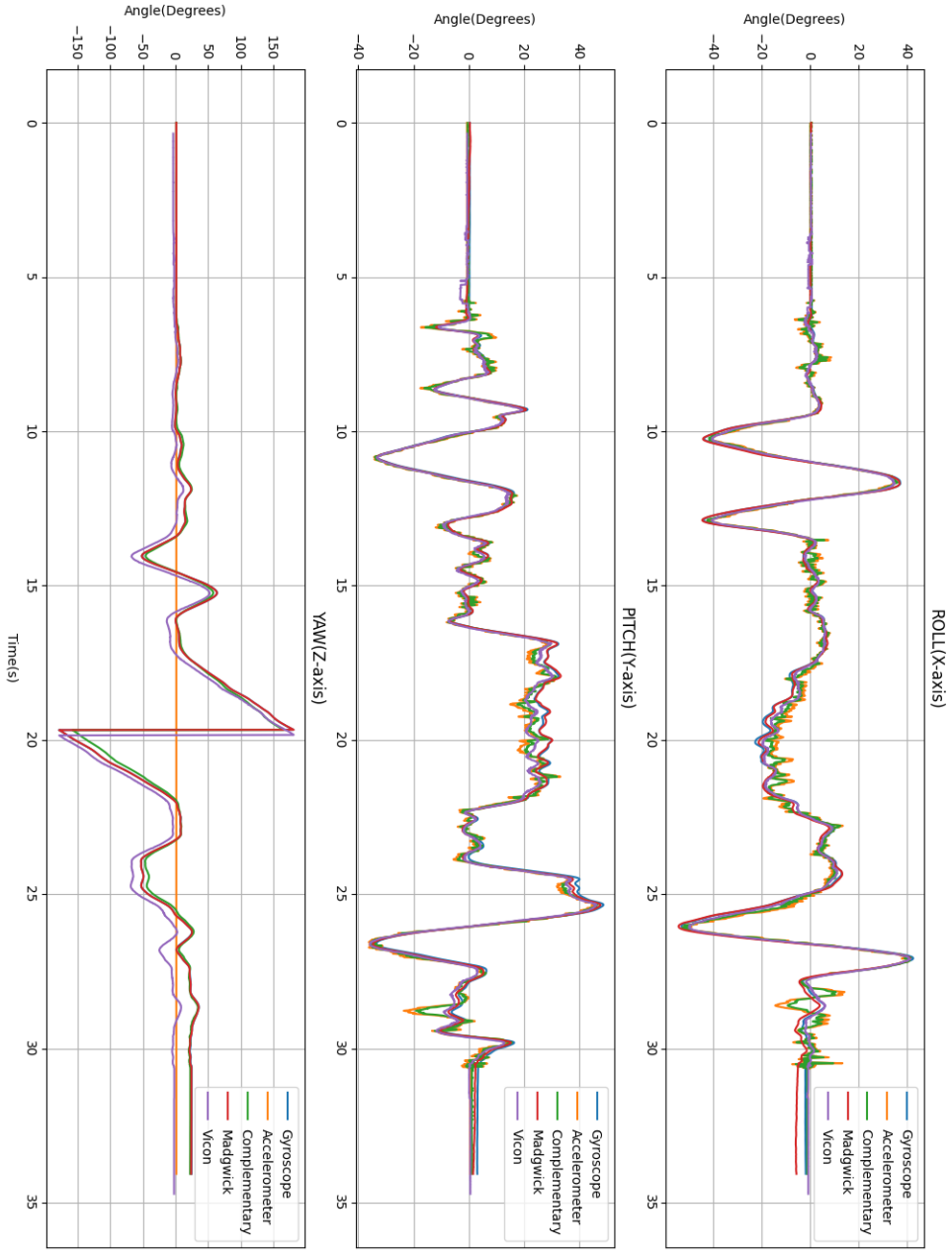

Fig. 3: Comparison of Attitude Estimation for dataset 3

4. TRAIN DATASET 4

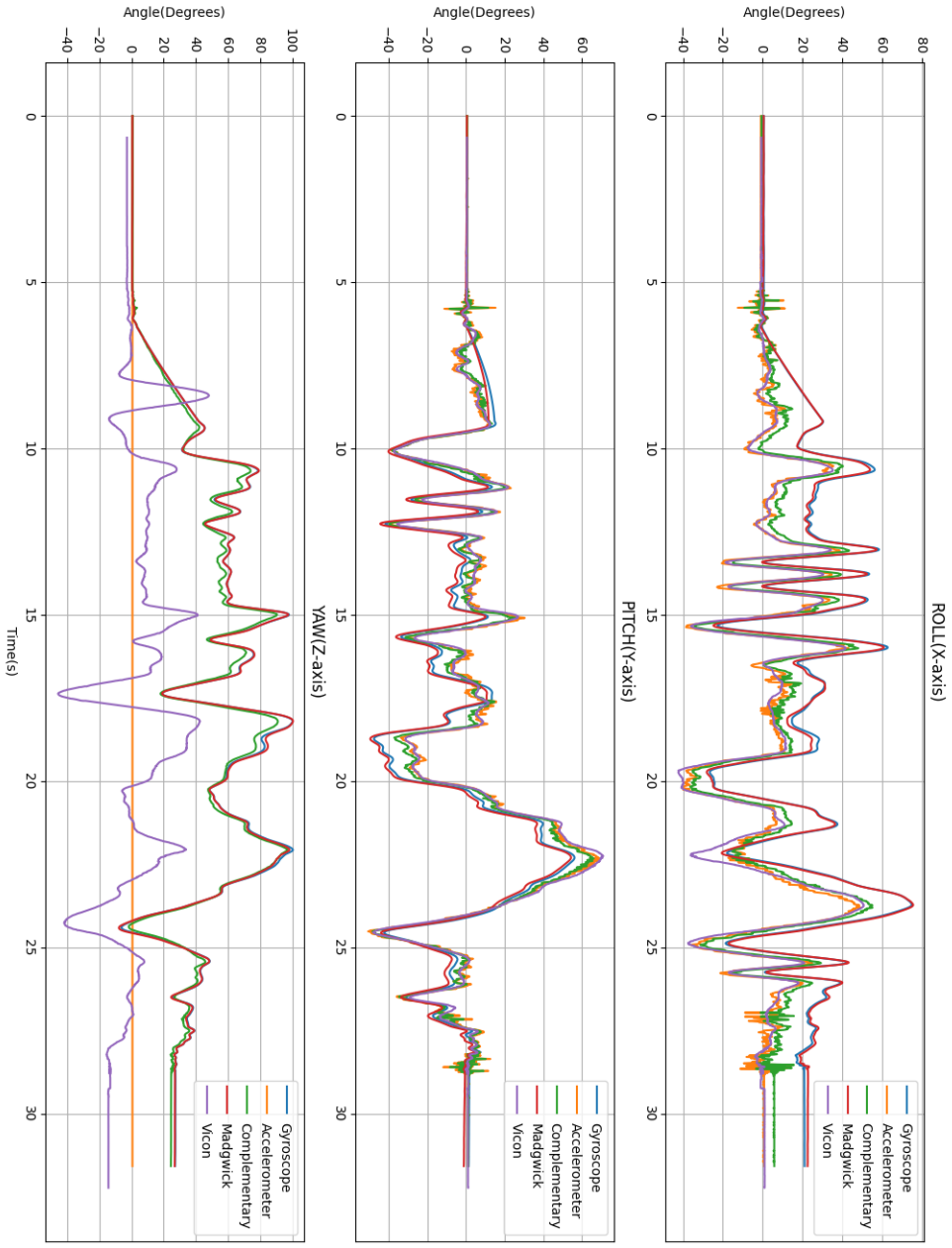

Fig. 4: Comparison of Attitude Estimation for dataset 4

5. TRAIN DATASET 5

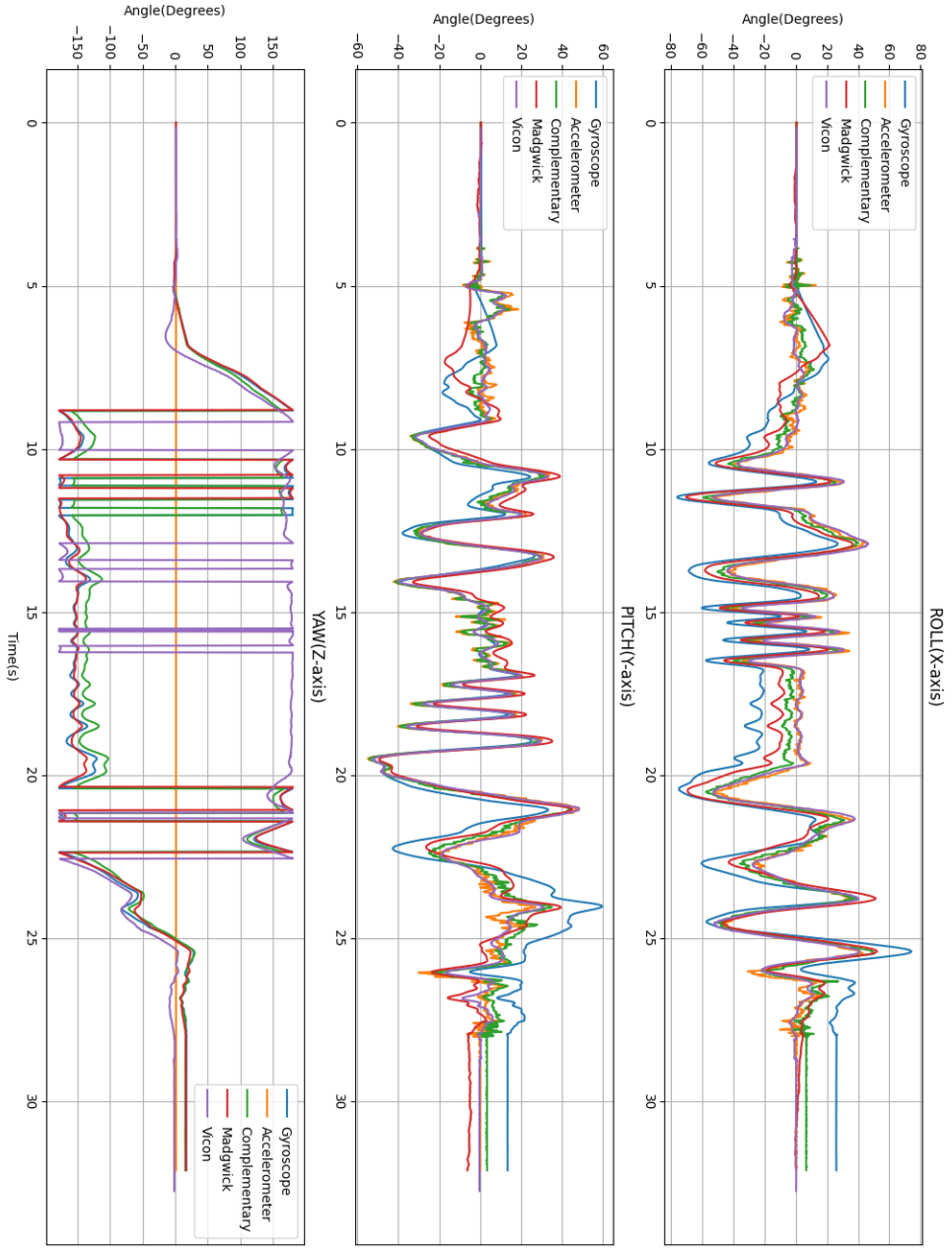

Fig. 5: Comparison of Attitude Estimation for dataset 5

6. TRAIN DATASET 6

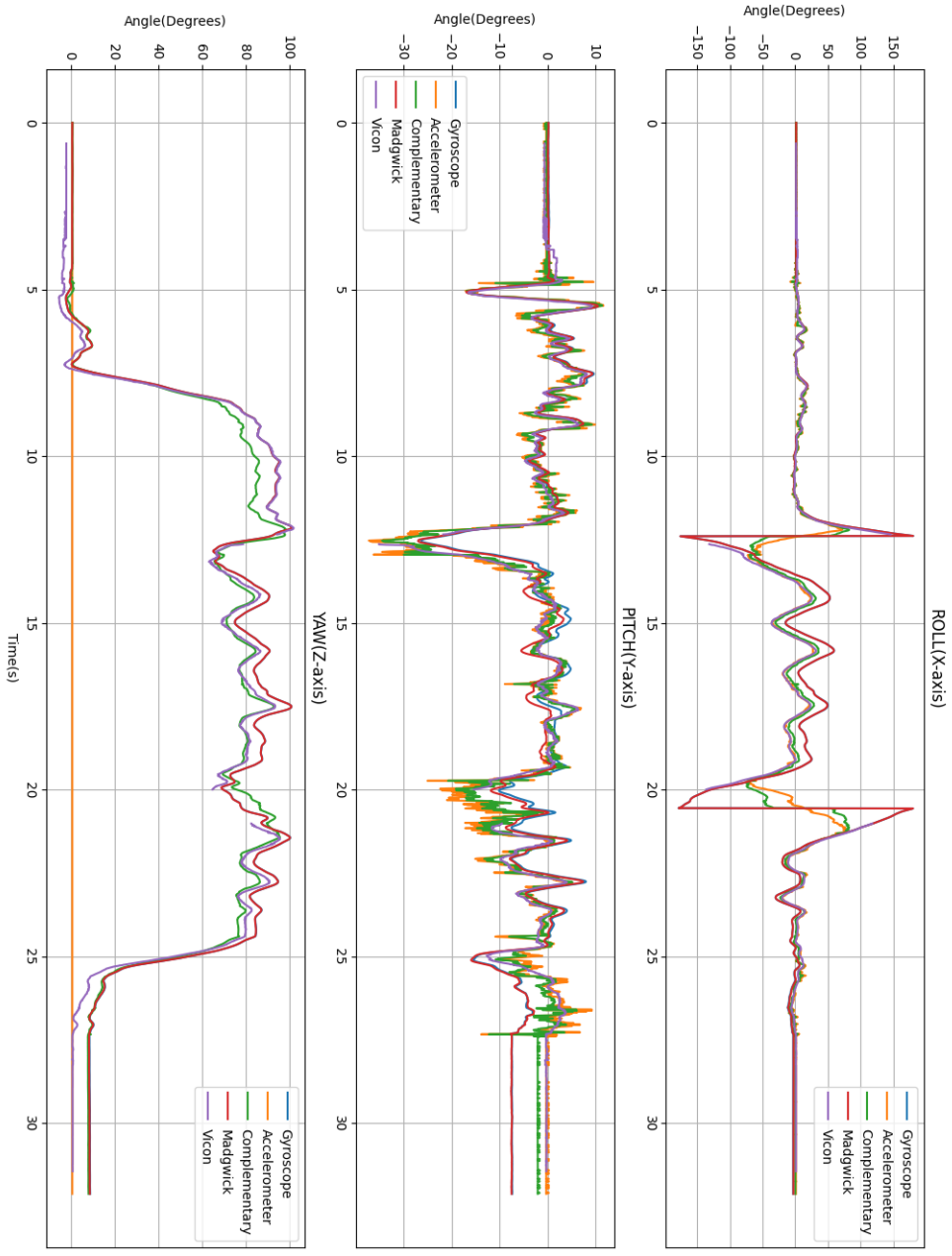

Fig. 6: Comparison of Attitude Estimation for dataset 6

7. TEST DATASET 7

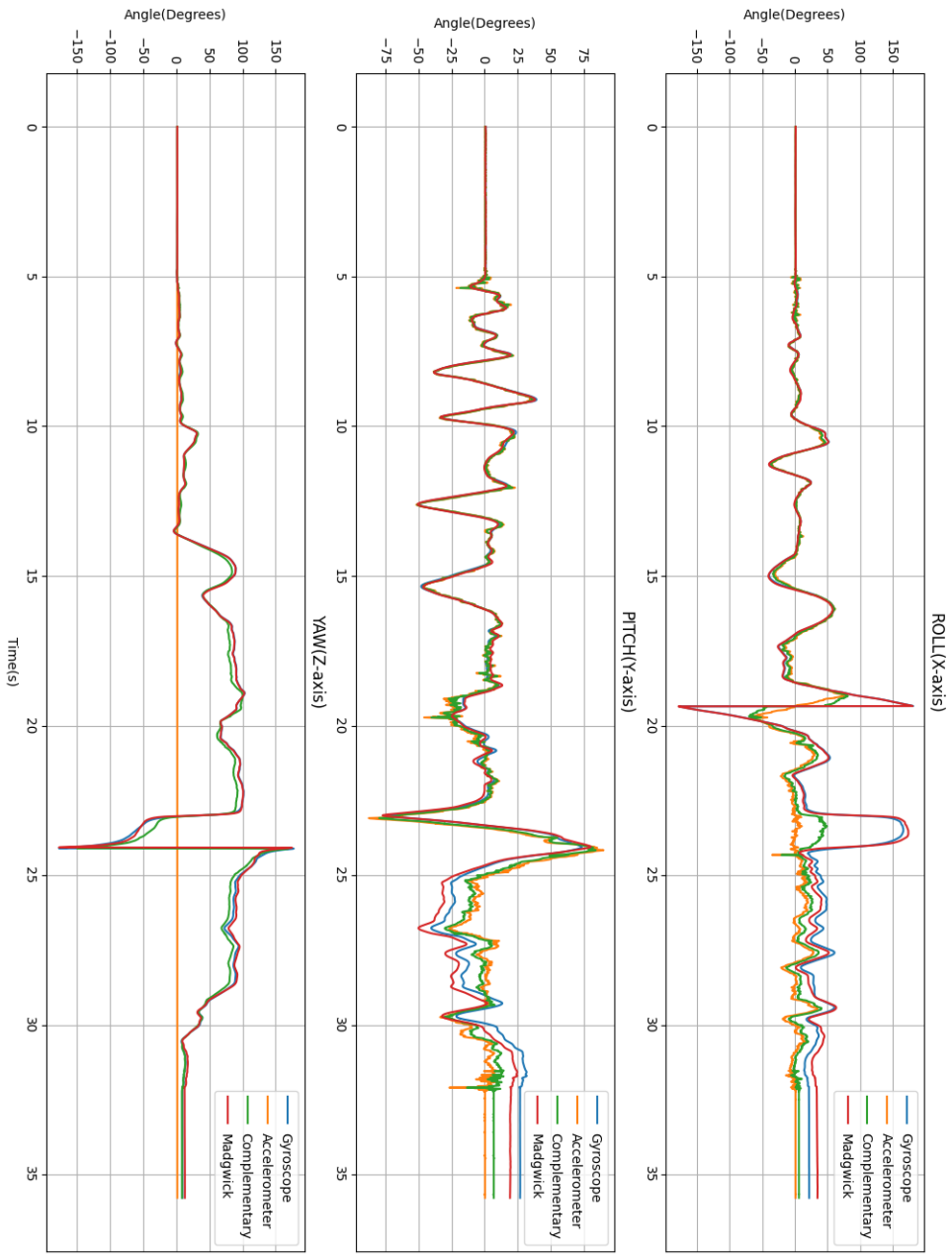

Fig. 7: Comparison of Attitude Estimation for dataset 7

8. TEST DATASET 8

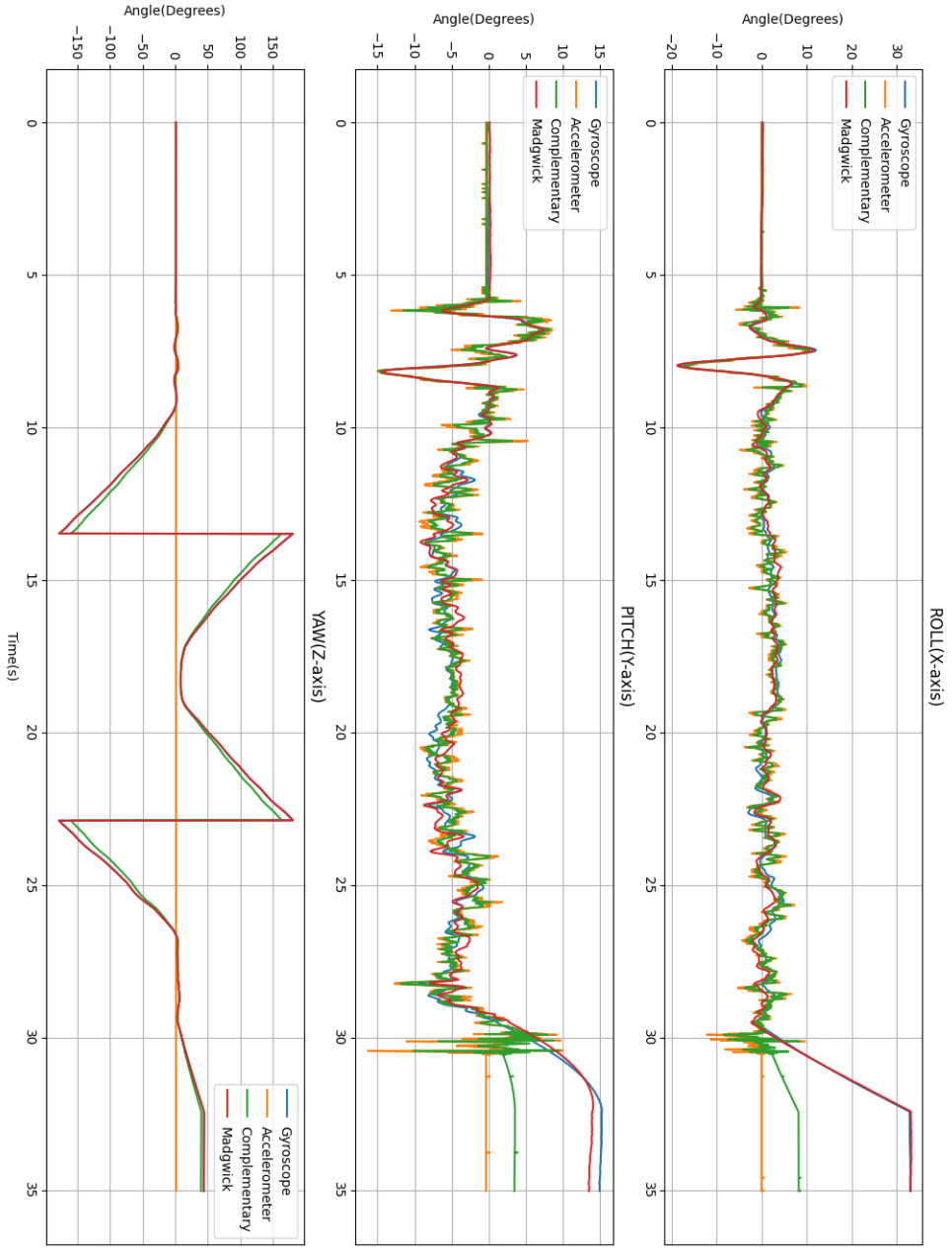

Fig. 8: Comparison of Attitude Estimation for dataset 8

9. TEST DATASET 9

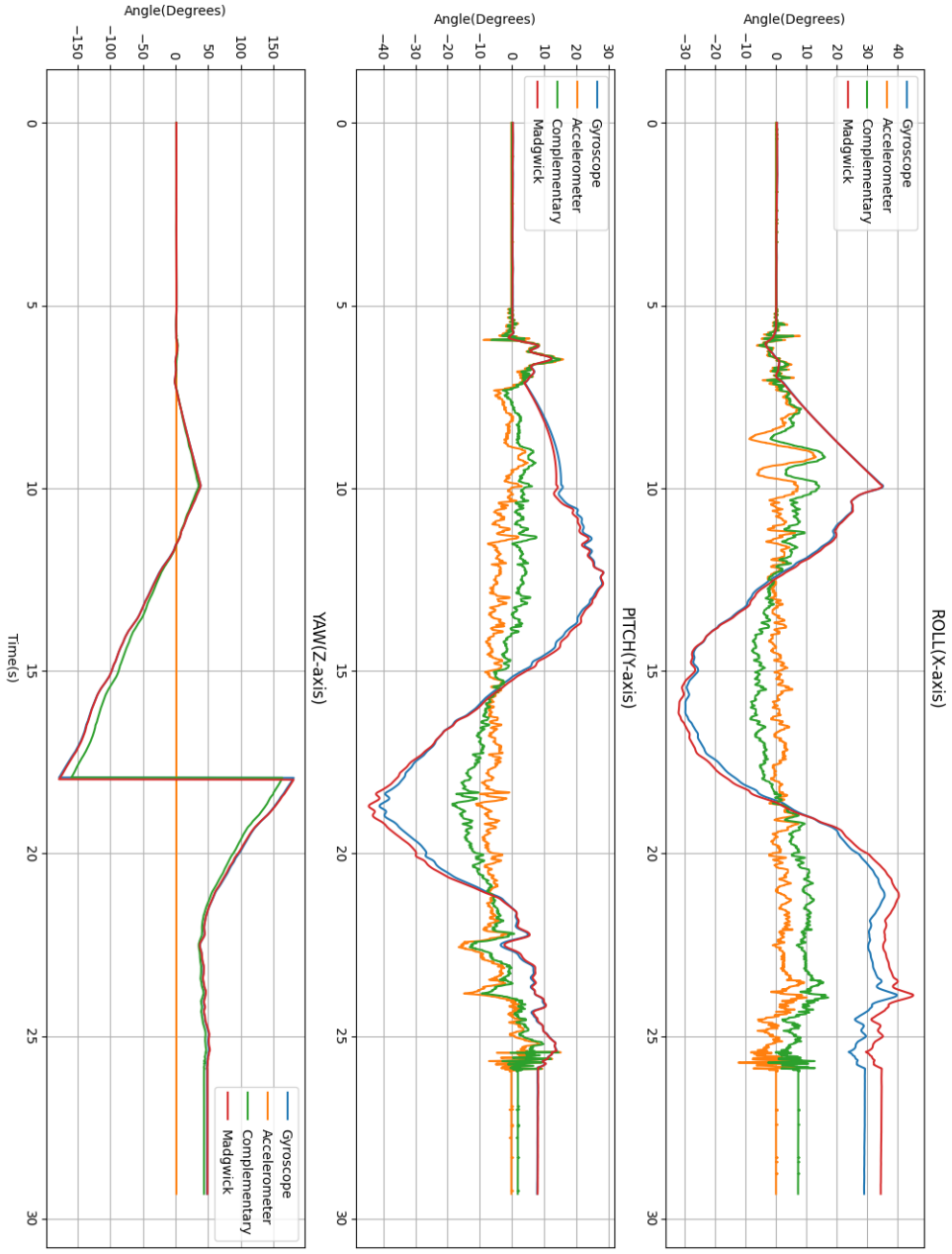

Fig. 9: Comparison of Attitude Estimation for dataset 9

10. TEST DATASET 10

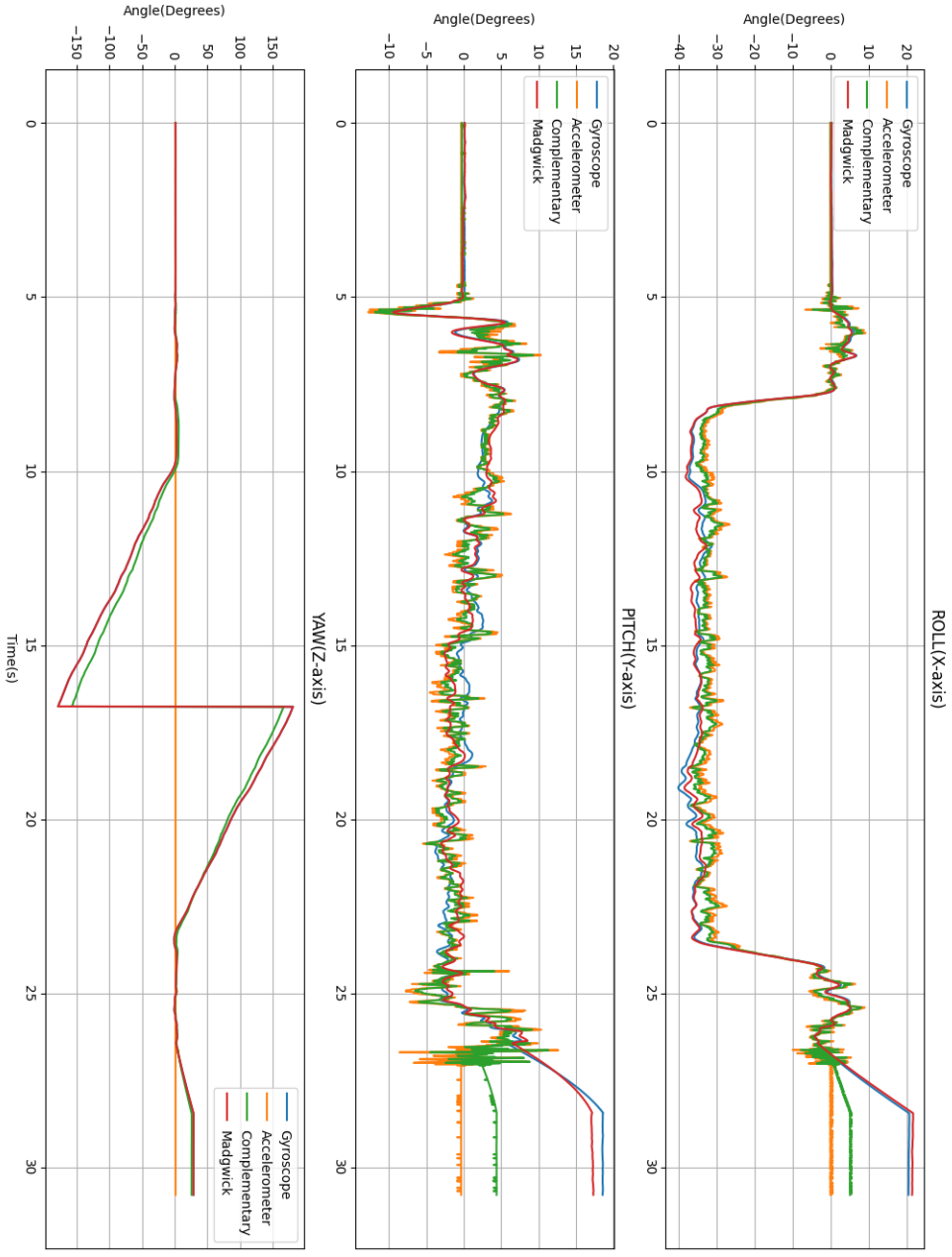

Fig. 10: Comparison of Attitude Estimation for dataset 10